Chemical Science

ROYAL SOCIETY OF CHEMISTRY

EDGE ARTICLE

View Article Online
View Journal | View Issue

Cite this: *Chem. Sci.*, 2024, **15**, 15725

All publication charges for this article have been paid for by the Royal Society of Chemistry

Received 6th July 2024
Accepted 23rd August 2024

DOI: 10.1039/d4sc04476b

rsc.li/chemical-science

$N_2H_4Zn(HC_3N_3O_3)$: exceptionally strong second harmonic generation and ultra-long phosphorescence†

Can Yang,‡[a] Yuwei Kang,‡[a] Xuefei Wang,[a] Jie Gou,[a] Yi Xiong,[a] Zece Zhu,[a] Ling Chen*[b] and Qi Wu*[a]

The discovery and designed synthesis of multifunctional materials is a leading pursuit in materials science. Herein, we report a novel hydro-isocyanurate, $N_2H_4Zn(HC_3N_3O_3)$, which combines strong second harmonic generation (SHG) and ultra-long room-temperature phosphorescence (RTP). The SHG intensity is the highest within the cyanurate system (13 × KDP), and RTP lifetime extends up to 448 ms, accompanied by a long-lasting afterglow visible to the naked eye for 1.2 s, surpassing most of the current metal–organic complexes. This advancement holds promise for the development of multifunctional optoelectronic devices, particularly leveraging second-harmonic generation (SHG) processes.

Introduction

The field of nonlinear optical (NLO) materials has been at the forefront of materials science, driving innovation in frequency conversion technologies such as second harmonic generation (SHG), which find wide applications in everyday life and industry.[1–5] On the other hand, materials that exhibit long-lived room-temperature phosphorescence (RTP) have been a great challenge. The rarity of materials that can stably maintain ultra-long RTP alongside strong SHG properties is primarily attributed to the complex interplay required between structural asymmetry for SHG activity and the delicate balance of energy states necessary for long-lived phosphorescence.[6–11] This dual functionality is highly desirable for applications ranging from secure optical communication to precise bio-imaging.[12–15]

Semi-organic NLO crystals emerge as a promising class of materials that combine the processability and tunability of organic components with the structural stability of their inorganic counterparts.[16–27] Herein, we report a novel semi-organic crystal, $N_2H_4Zn(HC_3N_3O_3)$, exhibiting exceptionally strong SHG and ultra-long RTP. The design rationale was to exploit the synergistic combination of a SHG-active $(HC_3N_3O_3)^{2-}$ building unit with the coordination tendency of Zn^{2+} and the unique neutral N_2H_4 ligand. This assembly not only results in a non-centrosymmetric (NCS) structure conducive to SHG activity but also facilitates efficient exciton transfer and intersystem crossing (ISC), essential for RTP. The SHG of $N_2H_4Zn(HC_3N_3O_3)$ is the strongest among that of metal cyanurates to date, surpassing that of KDP by a factor of 13, and it has an RTP lifetime of 448 ms, which is exceptionally long for metal complexes. Moreover, the material exhibits a visibly bright blue and green afterglow for up to 1.2 s. $N_2H_4Zn(HC_3N_3O_3)$ also shows a large bandgap of 5.38 eV, a thermal stability up to 250 °C, insensitivity to air, robust resistance to water as well as a notable birefringence (Δn) of 0.29 @ 546 nm, which further underscore its practicality. Finally, theoretical calculations and analyses are conducted to understand the observed phenomena, offering insights into the future design synthesis of multifunctional materials.

Results and discussion

Block-like single crystals of $N_2H_4Zn(HC_3N_3O_3)$, measuring up to 5 × 2 × 1 mm^3, were successfully synthesized using a hydrothermal stoichiometric reaction of $CH_6N_4{\cdot}HNO_3$, $ZnBr_2$, $C_3H_3N_3O_3$, and H_2O (Fig. S1†). The purity of the product was confirmed by using the fully assigned experimental powder X-ray diffraction (PXRD) data, which agree well with the single-crystal X-ray diffraction (SC-XRD) refinement results (Fig. S2†).

$N_2H_4Zn(HC_3N_3O_3)$ crystallizes in the monoclinic polar *Cc* space group (Tables S1–S4†). The CCDC number is 2331157. The structure of $N_2H_4Zn(HC_3N_3O_3)$ is a novel one, in which the Zn-centered tetrahedra are connected in a diamond-like topological three-dimensional (3D) framework (Fig. 1a) *via* the

[a]State /Key Laboratory of New Textile Materials and Advanced Processing Technologies, Wuhan Textile University, Wuhan 430200, China. E-mail: wuqi2011@whu.edu.cn

[b]Beijing Key Laboratory of Energy Conversion and Storage Materials, College of Chemistry, Beijing Normal University, Beijing 100875, China. E-mail: chenl@bnu.edu.cn

† Electronic supplementary information (ESI) available. CCDC 2331157. For ESI and crystallographic data in CIF or other electronic format see DOI: https://doi.org/10.1039/d4sc04476b

‡ These authors contributed equally.

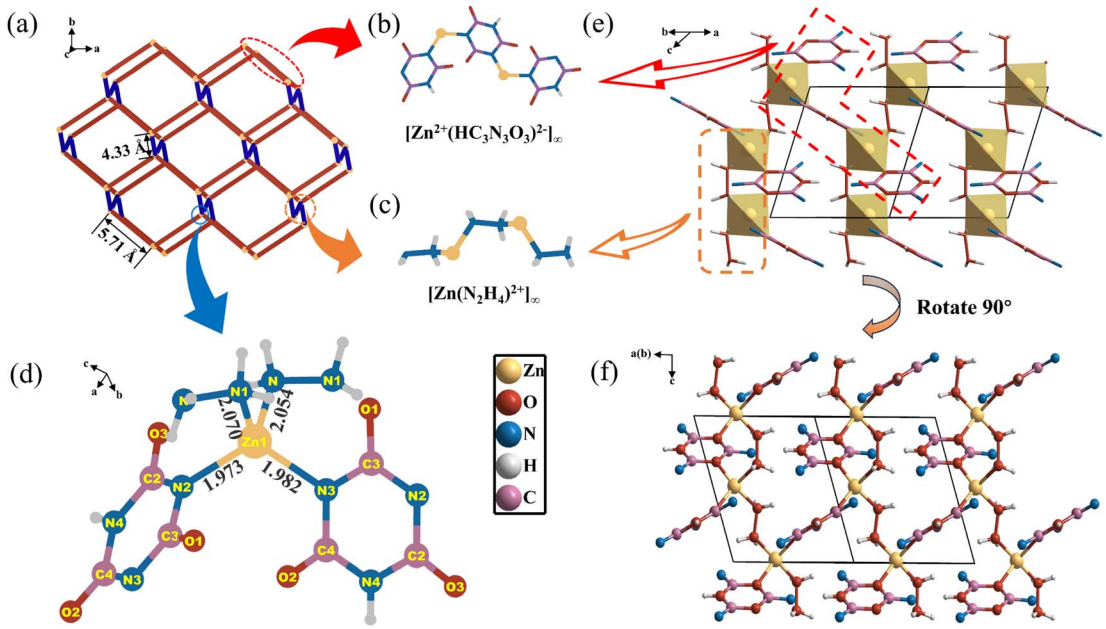

Fig. 1 (a) Highly diamond-like topology for $[Zn(HC_3N_3O_3)_2(N_2H_4)_2]$. (b) $[Zn^{2+}(HC_3N_3O_3)^{2-}]_\infty$ infinite chains. (c) $[Zn(N_2H_4)]_\infty{}^{2+}$ infinite chains. (d) The highly polarized $[Zn(HC_3N_3O_3)_2(N_2H_4)_2]$ tetrahedron. (e) The spatial arrangement of the polarized $[Zn(HC_3N_3O_3)_2(N_2H_4)_2]$ groups (the red dashed box represents $[Zn^{2+}(HC_3N_3O_3)^{2-}]_\infty$ infinite chains, and the orange dashed box represents $[Zn(N_2H_4)]_\infty{}^{2+}$ infinite chains). (f) The spatial arrangement of the polarized $[Zn(HC_3N_3O_3)_2(N_2H_4)_2]$ groups (obtained by rotating the f-diagram by 90°).

infinite anionic chains of ($[Zn^{2+}(HC_3N_3O_3)^{2-}]_\infty$) (Fig. 1b) extending along the *c*-axis that are interwoven with the infinite cationic chains of ($[Zn(N_2H_4)]_\infty{}^{2+}$) (Fig. 1c), together with hydrogen bonds (Table S5†). Within this network, the Zn–Zn distance (bridged by two $(HC_3N_3O_3)^{2-}$ rings) is 5.71 Å or 4.33 Å (bridged by two $[N_2H_4]$ molecules) (Fig. 1c). Each Zn1 atom is tetrahedrally coordinated to two distinct $(HC_3N_3O_3)^{2-}$ 6-MRs (Zn1–N1/3 bond lengths range from 1.973 Å to 1.982 Å) and two $[N_2H_4]$ molecules (Zn1–N4/5 bond lengths are in the range of 2.054 Å to 2.070 Å), resulting in the formation of the highly polarized $[Zn(HC_3N_3O_3)_2(N_2H_4)_2]$ tetrahedron (Fig. 1d). The Zn–N bond coordinated to the neutral hydrazine groups is slightly longer than that to the $(HC_3N_3O_3)^{2-}$ ring, which is mainly due to the mutual electrostatic attraction between Zn^{2+} and $(HC_3N_3O_3)^{2-}$ (and S3†). Considering the bond valence sum (BVS) calculation results (Table S6†) and the coordination environment of the Zn atom, the H atoms are added to N2 by geometry optimization, giving a hydro-isocyanuric anionic group, $(HC_3N_3O_3)^{2-}$. Within the $(HC_3N_3O_3)^{2-}$ group, the C–N bond lengths span a range from 1.357(4) to 1.374(4) Å. In contrast, the C–O bond varies in a slightly broader range, extending from 1.225(4) to 1.247(5) Å. Furthermore, the N–N bond within the $[N_2H_4]$ molecule is 1.457(4) Å. These bond distances agree well with those reported.[28,29]

In this structure, two differently oriented π-conjugated delocalized $(HC_3N_3O_3)^{2-}$ groups are present, and the dihedral angle between the two $(HC_3N_3O_3)^{2-}$ groups is 40.9° (Fig. S4†), while the intersection angle between two $[N_2H_4]$ molecules is 38° (Fig. S5†). The $[Zn(HC_3N_3O_3)_2(N_2H_4)_2]$ tetrahedron is highly polarized and constructs the diamond-like 3D network (Fig. 1e and f). Due to the absence of an inversion center in the polar *Cc* space group, all the polarized $[Zn(HC_3N_3O_3)_2(N_2H_4)_2]$ groups align uniformly facilitating significant anisotropy and effective superposition of 2nd nonlinear susceptibility.

The optical properties of $N_2H_4Zn(HC_3N_3O_3)$ were measured through infrared (IR), ultraviolet-visible (UV-vis) and photoluminescence (PL) spectroscopies. The IR stretching vibrations between N–H nitrogen and N–H···O at 2700–3500 and 792 cm^{-1} are observed. The vibrations at 1400–1700 cm^{-1} are attributed to $(HC_3N_3O_3)^{2-}$, and those at 1157 and 1374 cm^{-1} are attributed to C–O and C–N, respectively. These are the typical spectral features for cyanurate and isocyanurate derivatives (Fig. S6†). The UV-vis spectrum reveals a cutoff edge at 217 nm (E_g = 5.38 eV), the shortest in the hydro-isocyanurate family (Fig. 2a).

The birefringence (Δn) properties of $N_2H_4Zn(HC_3N_3O_3)$ were measured on an as-obtained crystal with a thickness of 4.71 μm by using a polarized optical microscope fitted with a Berek compensator, illuminated with a 589 nm monochromatic green light source. The extinction process, facilitated by optical compensation, yielded a retardation value of −1387.3 nm, giving a $\Delta n_{obv.}$ of 0.294 (Fig. S7†). The $\Delta n_{cal.}$ = 0.306 @ 589 nm in principle agrees well with this observation (Fig. 2b). The $\Delta n_{obv.}$ is comparable with those of other cyanurates and isocyanurates, such as $Pb_2Cd(HC_3N_3O_3)_2(OH)_2$ (0.291@800 nm), $LiRbHC_3N_3O_3\cdot 2H_2O$ (0.259@532 nm) and $NaRb_{0.84}Cs_{0.16}HC_3N_3O_3\cdot 2H_2O$ (0.238@532 nm) (Table S7†).[29–34] The large Δn of the title compound $N_2H_4Zn(HC_3N_3O_3)$ may arise mainly from the strong anisotropy and π–π conjugation interactions of the $(HC_3N_3O_3)^{2-}$ rings.

The particle-size-dependent SHG responses were measured by the Kurtz–Perry powder method utilizing a 1064 nm fundamental laser with KDP as a reference. The SHG responses of

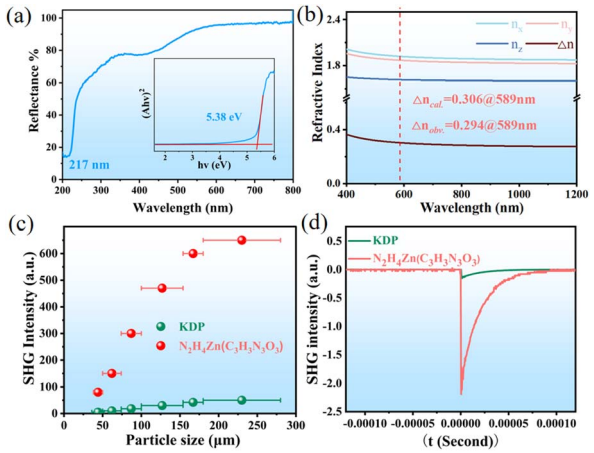

Fig. 2 Optical properties of $N_2H_4Zn(HC_3N_3O_3)$: (a) UV-vis diffuse reflectance spectrum; inset: the experimental band gap calculated with the Kubelka–Munk functional. (b) The calculated refractive indices. (c) Particle-size-dependent SHG intensity under 1064 nm laser irradiation (d) Oscilloscope traces of the SHG signals for polycrystalline samples with a particle size range of 180–280 μm.

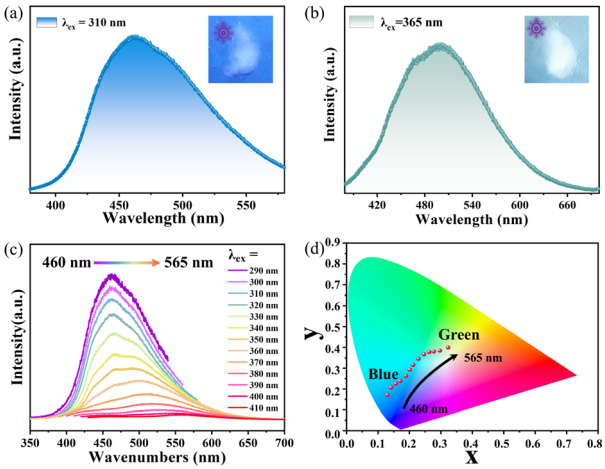

Fig. 4 The phosphorescence spectra of $N_2H_4Zn(HC_3N_3O_3)$. The emission spectra at (a) 310 nm; (b) 365 nm. (c) The emission spectrum from 290 to 410 nm. (d) CIE color chromaticity under excitation from 310 to 365 nm.

polycrystalline $N_2H_4Zn(HC_3N_3O_3)$ samples intensify with increasing particle size, reaching a plateau at approximately 180 μm, indicating a phase matching behavior (Fig. 2c). The maximal SHG response is 13 times that of KDP, the strongest intensity among cyanurates (Fig. 2d and Table S8†).[35–40]

The thermal stability and water and air resistance were studied. Unlike many isocyanurates, $N_2H_4Zn(HC_3N_3O_3)$ possesses an anhydrous 3D network structure and is thermally stable until 250 °C without undergoing decomposition (Fig. S8†). Moreover, after a six-month exposure to ambient air and humidity, the crystals remained unfazed, showing no signs of degradation or moisture absorption. As shown in Fig. 3, the color and weight of $N_2H_4Zn(HC_3N_3O_3)$ crystals remained unchanged after immersion in water for 10 days, and their the XRD patterns show no change before and after the immersion (Fig. S2†). Such a water treatment does not influence the green SHG light (532 nm) emission (Fig. 3).

The room-temperature photoluminescence properties were investigated. The fluorescence displays a broad emission band peaking at approximately 360 nm, corresponding to an excitation wavelength of 310 nm (Fig. S9†). Subsequent phosphorescence spectroscopy (Fig. 4c) indicated a dynamic red-shift in the emission peak position as the excitation wavelength was incrementally varied from 290 to 410 nm. This shift was observed to transition from around 460 nm to a range between 460 and 565 nm, marking emission adaptability. Fig. 4 depicts the dual-color emission capability; with an excitation wavelength of 310 nm, the emission peak is situated at around 460 nm indicative of blue light, while at 365 nm, the peak red-shifts to approximately 500 nm, corresponding to green light. This bioluminescence is corroborated by the 1931 International Commission on Radiation (CIE) chromaticity diagram (Fig. 4d). The naked-eye can distinctly perceive a persistent blue and green phosphorescent glow for about 1.2 s post-irradiation (Fig. 5d). The luminescence decay curves (Fig. 5a and b) further elucidate the multi-exponential decay behavior. The phosphorescence lifetimes are measured to be 448 ms and 428 ms for excitation wavelengths of 310 nm and 365 nm,

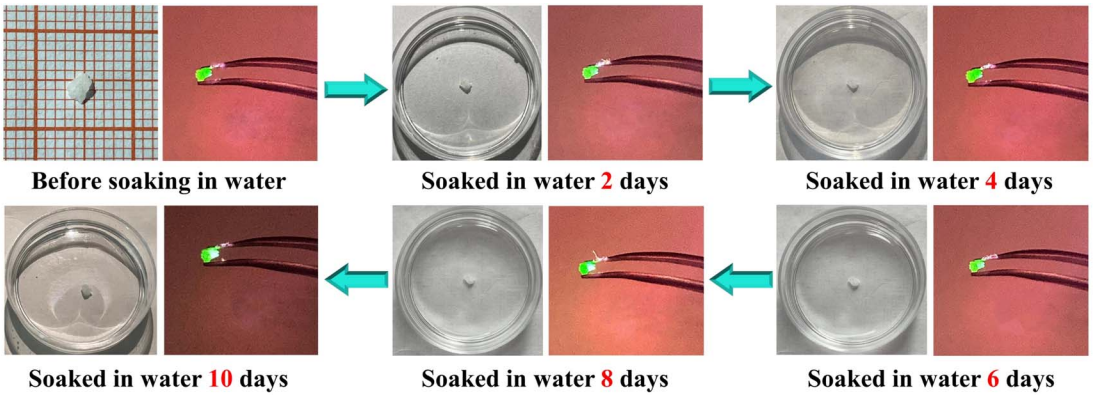

Fig. 3 Water resistance test of the as-synthesized $N_2H_4Zn(HC_3N_3O_3)$ crystal (the crystal emits green light at 532 nm when irradiated by using a 1064 nm laser).

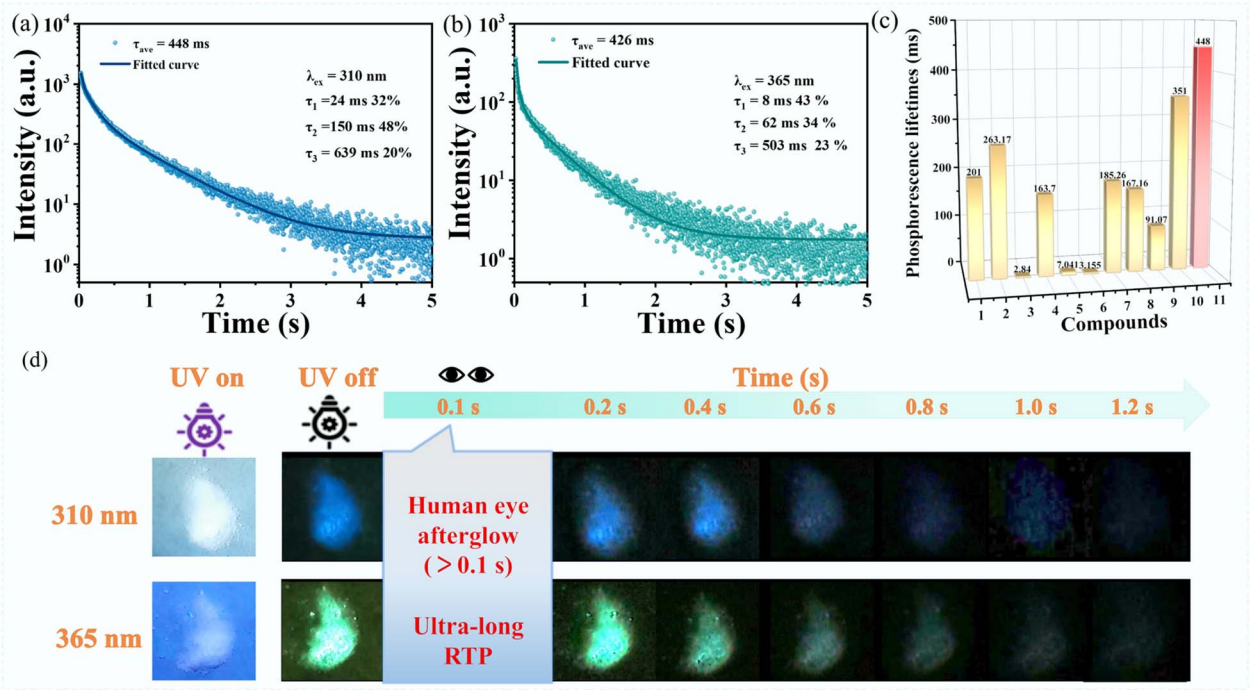

Fig. 5 The decay curves for $N_2H_4Zn(HC_3N_3O_3)$ at (a) 310 nm and (b) 365 nm. (C) The comparison of the phosphorescence lifetime of 11 selected compounds: $[Zn_4(HEDP)_2(TIMB)]\cdot H_2O$ (1), $(Ph_3S)_2ZnCl_4$ (2), $(Ph_3S)_2MnCl_4$ (3), $[NH_3Me]\cdot[Zn_2(HEDP)(TPA)_{0.5}(H_2O)_2]\cdot 2H_2O$ (4), $[Zn_5(BIPA)_4$-$MIM(OH)_2(H_2O)_2]$ (5), $[Zn_3(BIPA)_2(MIM)_3(OH)_2]\cdot 2H_2O$ (6), $Zn(HCOO)_2$(4,4′-bipy) (7), $ZnCl_2\cdot$R-2-MP (8), $ZnCl_2\cdot$S-2-MP (9), $Na_2Zn_2(C_9H_3O_6)_2(H_2O)_8\cdot 3H_2O$ (10) and the title compound (11). (d) Photographs of $N_2H_4Zn(HC_3N_3O_3)$ before and after removing the 310 and 365 nm UV lamp.

respectively, with an average lifetime exceeding 400 ms. This longevity is superior to most organic–Zn metal complexes (Table S9† and Fig. 5c).[41–47] Simultaneously, the temperature-dependent luminescence measurements have elucidated that the phosphorescence intensity of the sample escalates incrementally as the experimental temperature diminishes, corroborating the typical characteristics of phosphorescence phenomena (Fig. S10†).

To elucidate the relationship between the structure and properties of $N_2H_4Zn(HC_3N_3O_3)$, first-principles calculations were conducted using the CASTEP software package.[48] The electronic band structure indicates that the valence band maximum (VBM) is positioned at the *A* point, and the conduction band minimum (CBM) is located at the *M* point, signifying a direct band gap of 4.60 eV (Fig. S11†). Given the tendency for the band gap to be underestimated due to the discontinuity in the exchange-correlation energy functional, a scissor operator of 0.78 eV was employed for subsequent optical property calculations. The total and partial densities of states (DOS) reveal that the band gap is predominantly dictated by the interactions between C-2p and O-2p orbitals, as well as the C-2p and N-2p orbitals within the $[HC_3N_3O_3]^{2-}$ anionic group. The band associated with Zn-4s, 3d, and 3p states, and the N-2p state within the $[N_2H_4]$ group, are primarily located in the lower energy region ranging from −10 to −5 eV and contributes minimally around the Fermi level (Fig. S12†). The electron distribution curves of the VBM and CBM (Fig. 6a and d) suggest that the VBM is mainly composed of O-n states, while the CBM is mainly derived from the $(HC_3N_3O_3)^{2-}$-π* states. Thus, the organic component $(HC_3N_3O_3)^{2-}$ contributes to both the CBM and VBM by promoting n–π* leaps, which, according to the EI-Sayed rule, can effectively promote inter-system crossing (ISC) in favor of ultra-long room-temperature phosphorescence, which is consistent with the proposed organic emission mechanism.

Previous studies reveal that the N-2p orbitals in cyanuric 6-MRs can experience a down-shift in their band structure when the bridging N atoms coordinate with H or Zn atoms, leading to

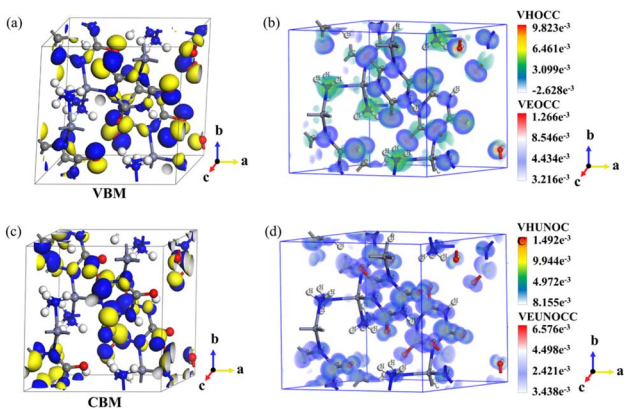

Fig. 6 The electron distribution profiles of $N_2H_4Zn(HC_3N_3O_3)$: the (a) VBM and (c) CBM. SHG weight factor analysis of the d_{11} component of the $N_2H_4Zn(HC_3N_3O_3)$ crystal (b) and (d).

an enlarged band gap for $Zn(H_2C_3N_3O_3)2\cdot 3H_2O$.[28] In the case of the title $N_2H_4Zn(HC_3N_3O_3)$ compound, one of the bridging N atoms forms a N–H bond, while the other two bridge N atoms coordinate with two distinct Zn atoms to form Zn–N bonds. This arrangement effectively diminishes the N-2p electronic states near the Fermi level, leading to a band gap of 5.38 eV.

The refractive index calculations revealed a distinct $n_z - n_y < n_y - n_x$ relationship, characterizing $N_2H_4Zn(HC_3N_3O_3)$ as a negative biaxial crystal. The calculated birefringence of 0.306@589 nm is in close agreement with the $\Delta n_{obv.}$ = 0.294@589 nm. The real-space atom-cutting calculations indicate that the $(HC_3N_3O_3)^{2-}$ anionic groups contribute primarily to the optical anisotropy with a substantial 0.340@589 nm. Meanwhile, Zn^{2+} and the $[N_2H_4]$ molecule have non-negligible but small contributions of 0.079 and 0.049@589 nm, respectively (Table S10†).

Utilizing the Kleinman approximation for point group m, $N_2H_4Zn(HC_3N_3O_3)$ has a set of five non-zero SHG tensors that were calculated to be $d_{12} = -7.6815$ pm V^{-1}, $d_{13} = -1.652$ pm V^{-1}, $d_{25} = -1.153$ pm V^{-1}, $d_{36} = 0.12$ pm V^{-1}, and $d_{11} = 8.017$ pm V^{-1}. The dominant d_{11} tensor is about 20-fold enhanced over the d_{36} of KDP. The SHG-weighted electron density analysis focusing on the d_{11} tensor was conducted to quantify the contributions from each structure building unit (Fig. 6). The SHG weight of the d_{11} component in the $N_2H_4Zn(HC_3N_3O_3)$ crystal (Fig. 6b and d) demonstrates that the virtual electron and virtual hole states are primarily driven by the $(HC_3N_3O_3)^{2-}$ ring, with Zn^{2+} and $[N_2H_4]$ contributing to a lesser extent.

The unoccupied molecular orbitals are attributed to the $(HC_3N_3O_3)^{2-}$ ring and the nitrogen atoms in the $[N_2H_4]$ molecule. This indicates that the SHG predominantly stems from the $(HC_3N_3O_3)^{2-}$ rings, with non-negligible contributions from the Zn^{2+} and $[N_2H_4]$ molecules, which contribute 79.60%, 10.50%, and 9.90% (Table S10†), respectively. This finding underscores the effective enhancement of the SHG responses in $N_2H_4Zn(HC_3N_3O_3)$ through the synergistic action of multiple chromophores.

Conclusions

In summary, a novel hydro-isocyanurate $N_2H_4Zn(HC_3N_3O_3)$ was discovered. This material exhibits an SHG response that is 13 × KDP, representing the strongest among cyanurates. The unique topological diamond-like framework not only achieves a short absorption edge at 217 nm and a large birefringence of $\Delta n_{obv.}$ = 0.294@589 nm, but also facilitates an exceptionally high thermal stability, and strong water resistance. Moreover, such a topological diamond-like framework also displays tunable multicolor room-temperature phosphorescence and a long RTP lifetime of 448 ms, accompanied by a long-lasting afterglow visible to the naked eye for 1.2 s, which is the longest among SHG-based metal–organic complexes, highlighting the material's potential for diverse applications in optoelectronics and beyond.

Data availability

Data available in the ESI† include the experimental section and additional tables and figures.

Author contributions

Can Yang and Yuwei Kang synthesized and characterized the title compound, and completed the writing of this manuscript. Qi Wu and Ling Chen provided experimental ideas and revised the manuscript. Xuefei Wang and Jie Gou participated in the data analysis and discussion of the article. Yi Xiong provided assistance in the characterization of compounds. Zece Zhu provided a discussion of the testing and data analysis of phosphorescence. The manuscript was written through contributions of all authors.

Conflicts of interest

There are no conflicts to declare.

Acknowledgements

This work was supported by the National Natural Science Foundation of China (no. 22275052). The authors would like to thank Chensheng Lin, Jun Zhang, Yuchao Li and Xingxing Jiang for their help in the theoretical calculations.

Notes and references

1 P. Becker, *Adv. Mater.*, 1998, **10**, 979–992.
2 D. Cyranoski, *Nature*, 2009, **457**, 953–956.
3 D. F. Eaton, *Science*, 1991, **253**, 281–287.
4 N. Savage, *Nat. Photonics*, 2007, **1**, 83–85.
5 R. Ikuta, Y. Kusaka, T. Kitano, H. Kato, T. Yamamoto, M. Koashi and N. Imoto, *Nat. Commun.*, 2011, **2**, 537.
6 C. Wu, T. Wu, X. Jiang, Z. Wang, H. Sha, L. Lin, Z. Lin, Z. Huang, X. Long and M. G. Humphrey, *J. Am. Chem. Soc.*, 2021, **143**, 4138–4142.
7 H. Liu, H. Wu, Z. Hu, J. Wang, Y. Wu and H. Yu, *J. Am. Chem. Soc.*, 2023, **145**, 12691–12700.
8 Y. Yang, Y. Xiao, B. Li, Y.-G. Chen, P. Guo, B. Zhang and X.-M. Zhang, *J. Am. Chem. Soc.*, 2023, **145**, 22577–22583.
9 S. Fang, H. Li, Y. Xie, H. Li, Y. Wang and Y. Shi, *Small*, 2021, **17**, 2103831.
10 Z. Zhu, L. Zeng, W. Li, W. Xu and D. Tian, *ACS Sustainable Chem. Eng.*, 2022, **10**, 16752–16759.
11 Z. Qi, B. Zhou and D. Yan, *Mater. Chem. Front.*, 2023, **7**, 3475–3493.
12 X. Kang and M. Zhu, *Chem. Soc. Rev.*, 2019, **48**, 2422–2457.
13 L. Chen, L. Yu, Y. Liu, H. Xu, W. Li, F. Wang, J. Zhu, K. Yi, L. Ma and H. Xiao, *ACS Sens.*, 2023, **8**, 3104–3115.
14 Z. Zhu, L. Zeng, W. Li, D. Tian and W. Xu, *ACS Sustainable Chem. Eng.*, 2021, **9**, 17420–17426.
15 S. Xu, R. Chen, C. Zheng and W. Huang, *Adv. Mater.*, 2016, **28**, 9920–9940.
16 J. Lu, X. Liu, M. Zhao, X. B. Deng and L. M. Wu, *J. Am. Chem. Soc.*, 2021, **143**, 3647–3654.
17 F. Ge, B.-H. Li, P. Cheng, G. Li, Z. Ren, J. Xu and X.-H. Bu, *Angew. Chem., Int. Ed.*, 2022, **61**, e202115024.
18 D. Lin, M. Luo, C. Lin, F. Xu and N. Ye, *J. Am. Chem. Soc.*, 2019, **141**, 3390–3394.

19 Y. Li, W. Huang, Y. Zhou, X. Song, J. Zheng, H. Wang, Y. Song, M. Li, J. Luo and S. Zhao, *Angew. Chem., Int. Ed.*, 2023, **62**, e202215145.
20 L. Liu, Z. Bai, L. Hu, D. Wei, Z. Lin and L. Zhang, *J. Mater. Chem. C*, 2021, **9**, 7452–7457.
21 Y. Liu, Y. P. Gong, S. Geng, M. L. Feng, D. Manidaki, Z. Deng, C. C. Stoumpos, P. Canepa, Z. Xiao and W. X. Zhang, *Angew. Chem., Int. Ed.*, 2022, **61**, e202208875.
22 X. Meng, X. Zhang, Q. Liu, Z. Zhou, X. Jiang, Y. Wang, Z. Lin and M. Xia, *Angew. Chem.*, 2023, **135**, e202214848.
23 Y. Kang, C. Yang, J. Gou, Y. Zhu, Q. Zhu, W. Xu and Q. Wu, *Angew. Chem.*, 2024, **136**, e202402086.
24 K. Wan, B. Tian, Y. Zhai, Y. Liu, H. Wang, S. Liu, S. Li, W. Ye, Z. An and C. Li, *Nat. Commun.*, 2022, **13**, 5508.
25 H. Liu, Y. Gao, J. Cao, T. Li, Y. Wen, Y. Ge, L. Zhang, G. Pan, T. Zhou and B. Yang, *Mater. Chem. Front.*, 2018, **2**, 1853–1858.
26 J. Yu, H. Ma, W. Huang, Z. Liang, K. Zhou, A. Lv, X.-G. Li and Z. He, *JACS Au*, 2021, **1**, 1694–1699.
27 H. Ma, Q. Peng, Z. An, W. Huang and Z. Shuai, *J. Am. Chem. Soc.*, 2018, **141**, 1010–1015.
28 D. Wang, X. Zhang, F. Liang, Z. Hu and Y. Wu, *Dalton Trans.*, 2021, **50**, 5617–5623.
29 D. Lin, M. Luo, C. Lin, F. Xu and N. Ye, *J. Am. Chem. Soc.*, 2019, **141**, 3390–3394.
30 J. Lu, Y.-K. Lian, L. Xiong, Q.-R. Wu, M. Zhao, K.-X. Shi, L. Chen and L.-M. Wu, *J. Am. Chem. Soc.*, 2019, **141**, 16151–16159.
31 N. Wang, F. Liang, Y. Yang, S. Zhang and Z. Lin, *Dalton Trans.*, 2019, **48**, 2271–2274.
32 X. Meng, F. Liang, K. Kang, J. Tang, T. Zeng, Z. Lin and M. Xia, *Inorg. Chem.*, 2019, **58**, 11289–11293.
33 X. Meng, K. Kang, F. Liang, J. Tang, Z. Lin, W. Yin and M. Xia, *Dalton Trans.*, 2020, **49**, 1370–1374.
34 X. Meng, K. Kang, F. Liang, J. Tang, W. Yin, Z. Lin and M. Xia, *Inorg. Chem. Front.*, 2020, **7**, 3674–3686.
35 M. Xia, M. Zhou, F. Liang, X. Meng, J. Yao, Z. Lin and R. Li, *Inorg. Chem.*, 2018, **57**, 32–36.
36 X. Meng, X. Zhang, Q. Liu, Z. Zhou, X. Jiang, Y. Wang, Z. Lin and M. Xia, *Angew. Chem.*, 2023, **135**, e202214848.
37 Y. Song, D. Lin, M. Luo, C. Lin, Q. Chen and N. Ye, *Inorg. Chem. Front.*, 2020, **7**, 150–156.
38 Y. Chen, C. Hu, Z. Fang and J. Mao, *Inorg. Chem. Front.*, 2021, **8**, 3547–3555.
39 M. Aibibula, L. Wang and S. Huang, *ACS Omega*, 2019, **4**, 22197–22202.
40 X. Meng, F. Liang, J. Tang, K. Kang, Q. Huang, W. Yin, Z. Lin and M. Xia, *Eur. J. Inorg. Chem.*, 2019, **2019**, 2791–2795.
41 F.-Y. Cao, H.-H. Liu, Y. Mu, Z.-Z. Xue, J.-H. Li and G.-M. Wang, *J. Phys. Chem. Lett.*, 2022, **13**, 6975–6980.
42 Z. Luo, Y. Liu, Y. Liu, C. Li, Y. Li, Q. Li, Y. Wei, L. Zhang, B. Xu and X. Chang, *Adv. Mater.*, 2022, **34**, 2200607.
43 H. Liu, W. Ye, Y. Mu, H. Ma, A. Lv, S. Han, H. Shi, J. Li, Z. An and G. Wang, *Adv. Mater.*, 2022, **34**, 2107612.
44 D. Li, X. Yang and D. Yan, *ACS Appl. Mater. Interfaces*, 2018, **10**, 34377–34384.
45 Y. J. Ma, X. Fang, G. Xiao and D. Yan, *Angew. Chem., Int. Ed.*, 2022, **61**, e202114100.
46 Y. Wang, C. Wang, M. Sun, P. Zhao, X. Fang, J. Zhang, Y. Guo and G. Zhao, *Adv. Opt. Mater.*, 2024, **12**, 2301843.
47 H. Zhang, Y. Yan, G. Qiao and J. Li, *Inorg. Chem. Commun.*, 2019, **104**, 119–123.
48 S. J. Clark, M. D. Segall, C. J. Pickard, P. J. Hasnip, M. I. Probert, K. Refson, M. C. Payne and Z. Krist, *Cryst. Mater.*, 2005, **220**, 567–570.